

Gamow-Siegert functions and Darboux-deformed short range potentials¹

Nicolás Fernández-García and Oscar Rosas-Ortiz

Departamento de Física, Cinvestav, AP 14-740, 07000 México D F, Mexico

Abstract

Darboux-deformations of short range one-dimensional potentials are constructed by means of Gamow-Siegert functions (resonance states). Results include both Hermitian and non-Hermitian short range potentials which are exactly solvable. As illustration, the method is applied to square wells and barriers for which the transmission coefficient is a superposition of Fock-Breit-Wigner distributions. Resonance levels are calculated in the long lifetime limit by means of analytical and numerical approaches. The new complex potentials behave as an optical device which both refracts and absorbs light waves.

1 Introduction

Gamow-Siegert functions are solutions of the Schrödinger equation associated to complex eigenvalues and fulfilling purely outgoing conditions [1, 2]. Although these functions are not square-integrable, they are used to model physical phenomena as resonances which, incidentally, are defined experimentally better than theoretically. Some approaches extend the formalism of quantum theory so that resonant states can be defined in a precise form. For instance, in the formulation of the rigged Hilbert space, Gamow vectors are studied in the framework of the nuclear spectral theorem [3, 4]. Resonances are also connected with the point spectrum of complex-scaled Hamiltonians [5].

In a different context, complex eigenvalues of Hermitian Hamiltonians have been used to implement Darboux (supersymmetric) transformations in quantum mechanics [6–9] (see also the discussion on ‘atypical models’ in [10]). The transformed Hamiltonians include non-Hermitian ones, for which the point spectrum sometimes has a single complex eigenvalue [7, 8]. This last result, combined with appropriate squeezing operators [11], could be in connection with the complex-scaling technique [8]. In general, supersymmetric transformations constitute a powerful tool in quantum mechanics [10]. As far as we know, however, the study of Darboux-deformations of potentials with resonances is still missing in the literature.

In this paper we deal with one-dimensional short range potentials and their resonances. As usual, the complex energy eigenvalue $\epsilon = E - i\Gamma/2$ will be taken as a compound of the

¹NOTICE: this is the author’s version of a work that was accepted for publication in *Annals of Physics*. Changes resulting from the publishing process, such as peer review, editing, corrections, structural formatting, and other quality control mechanisms may not be reflected in this document. Changes may have been made to this work since it was submitted for publication. A definitive version was subsequently published in *Annals of Physics* **323** (2008) 1397-1414 [DOI:10.1016/j.aop.2007.11.002]

resonance E and the inverse of the lifetime Γ . It will be shown that resonances can be labelled by a positive integer, according with their closeness to the scattering threshold. This integer thus indicates the ‘grade of excitation’ of the related state: the ‘ground resonance’ will correspond to the least excited Gamow-Siegert state and so on. We shall use these solutions to implement Darboux transformations; in this way several exactly solvable complex and real potentials will be constructed. As we are going to see, the Darboux-Gamow deformation which is produced on the initial potential strongly depends on the ‘excitation’ of the transformation function. Moreover, the complex potentials so derived behave as an optical device which both refracts and absorbs light waves. Such a behaviour will be illustrated with the simplest short range one-dimensional models: square wells and barriers.

In sections 2 and 3 we present general analytical conditions to construct Gamow-Siegert functions for one-dimensional short-range potentials and the corresponding Darboux-deformations. In Section 4, we will express the transmission coefficient T as a superposition of Fock-Breit-Wigner (Lorentzian) distributions for square well potentials. As we shall see, each one of the bell shaped peaks arises since T has a pole at $\epsilon \in \mathbb{C}$, which is a complex eigenvalue of the square well. The Darboux-Gamow deformations of these simple wells give rise to complex potentials $\tilde{V} = \tilde{V}_R + i\tilde{V}_I$ for which the function \tilde{V}_I shows multiple changes of sign, thus each \tilde{V} emits and absorbs flux at the same time. All the new potentials of this section have square-integrable functions which represent bound states associated with eigenvalues in the point spectrum. In Section 5 the case of square barriers is analyzed. We shall show that Gamow-Siegert functions also lead to a transmission coefficient which is a sum of Fock-Breit-Wigner distributions. In this case, ‘haired’ square barriers appear as a consequence of double Darboux-Gamow deformations for which the number of hairs is in close connection with the level of excitation of the transformation function. Finally, in Section 6 we finish the paper with some concluding remarks. A short appendix is included in order to present further information which, although important, can be delayed.

2 Gamow-Siegert states and one-dimensional short range potentials

Let us consider the Schrödinger equation for a stationary, short range potential $V(x)$, defined on the straight line \mathbb{R} ($\hbar/2m = 1$):

$$Hu(x, \epsilon) = -u''(x, \epsilon) + V(x)u(x, \epsilon) = \epsilon u(x, \epsilon). \quad (1)$$

In the sequel, we shall assume that $V(x)$ is characterized by a strength V_0 and a cutoff parameter $\zeta > 0$ such that $V(x) = 0$ if $|x| > \zeta$. A bar over $z \in \mathbb{C}$ stands for complex conjugation (\bar{z}) while z_R, z_I , denote real and imaginary parts respectively. In general, $I_+(z)$ denotes the upper half of the z -plane ($z_I > 0$) and $I_-(z)$ the lower half plane. Whenever there is no confusion we use the shortcut notation $f \equiv f(x, \epsilon, \dots)$, keeping implicit the dependence of f on x, ϵ , and other possible variables.

It is useful to write the derivative of the logarithm of u as the complex function $\beta(x, \epsilon)$:

$$\beta := -\frac{d}{dx} \ln u. \quad (2)$$

Let us also write $u = \Phi e^{i\Xi}$, with $\Phi(x)$ and $\Xi(x)$ real functions defined as

$$\Phi = \Phi_0 \exp\left(-\int \beta_R dx\right), \quad \Xi = -\int \beta_I dx + \Xi_0 \quad (3)$$

where Φ_0 and Ξ_0 are integration constants included to fix the amplitude Φ and phase Ξ respectively. Thereby, the current density

$$j = i(\bar{u}'u - \bar{u}u') \quad (4)$$

can be written as

$$j = 2\Xi'|u|^2 = -2\beta_I|u|^2 = v\rho. \quad (5)$$

Hence, $-2\beta_I$ represents the flux velocity v , which plays an important role in the description of Gamow-Siegert functions as well as in the Darboux transformations we are going to implement.

2.1 Asymptotic behaviour of the general solution

The general solution of (1) for $|x| > \zeta$ can be written in terms of ingoing and outgoing waves:

$$u(x < -\zeta) = Ie^{ikx} + Le^{-ikx}, \quad u(x > \zeta) = Ne^{-ikx} + Se^{ikx} \quad (6)$$

where coefficients I, L, N, S , depend on the potential parameters ζ, V_0 , and the incoming energy $k^2 = \epsilon$. Among these solutions, we are interested in those which are purely outgoing waves. The appropriate boundary condition may be written

$$\lim_{x \rightarrow \pm\infty} (u' \mp ik u) = \lim_{x \rightarrow \pm\infty} \{(-\beta \mp ik) u\} = 0. \quad (7)$$

Thus, the second term in each of the functions (6) must dominate over the first one. For such states, equation (4) takes the form:

$$j = \pm(\bar{k} + k)|u|^2, \quad \text{at } x \gtrless \pm\zeta. \quad (8)$$

If $\epsilon = E$, then k is either pure imaginary or real according to E is negative or positive. If we assume that the potential admits negative energies, we get $k_{\pm} = \pm i\sqrt{|E|}$ and (8) vanishes (the flux velocity v is zero outside the interaction zone). The solutions $\psi_E^{(+)}$, connected to k_+ , are not of our immediate interest because they are bounded (indeed, the adequate values of k_+ produce square-integrable functions in \mathbb{R}). On the other hand, *antibound states* $\psi_E^{(-)}$ increase exponentially as $|x| \rightarrow +\infty$ and represent resonances under very special conditions (see e.g. [12]). However, these states will not be considered here since they do not exist for arbitrary short range potentials. To exhaust the cases of a real

eigenvalue ϵ , let us take now $E > 0$. The outgoing condition (7) drops the interference term in the density

$$\rho(x; t) = |N|^2 + |S|^2 + 2|\overline{N}S| \cos(2\kappa x + \text{Arg } S/N), \quad x > \zeta, \quad (9)$$

so that $\rho = |S|^2$ is not an integrable function in neither space nor time (similar expressions hold for $x < -\zeta$). Remark that flux velocity is not zero outside the interaction zone ($|v| = 2\sqrt{E}$). Thereby, $E > 0$ provides outgoing waves at the cost of a net outflow $j \neq 0$. To get solutions which are more appropriate for this nontrivial j , we shall consider complex eigenvalues ϵ .

2.2 Resonances

From the discussion of the previous section it follows that, in general, ϵ must be complex. We shall write

$$\epsilon = E - \frac{i}{2}\Gamma, \quad \epsilon_R = k_R^2 - k_I^2, \quad \epsilon_I = 2k_R k_I \quad (10)$$

where $\epsilon = (k_R + ik_I)^2$. According to (7), the boundary condition for β reads now

$$\lim_{x \rightarrow \pm\infty} \{-\beta \pm (k_I - ik_R)\} = 0 \quad (11)$$

so that the flux velocity is $v_+ = +2k_R$ for $x > \zeta$ and $v_- = -2k_R$ for $x < -\zeta$. Hence, the ‘‘correct’’ direction in which the outgoing waves move is given by $k_R > 0$. In this case, the density

$$\rho(x; t) \equiv |u(x, t)|^2 = e^{-\Gamma t} |u(x)|^2, \quad \lim_{x \rightarrow \pm\infty} \rho(x; t) = e^{-\Gamma(t-x/v_{\pm})} \quad (12)$$

can be damped by taking $\Gamma > 0$. Thereby, $k_I \neq 0$ and $k_R \neq 0$ have opposite signs. Since $k_R > 0$ has been previously fixed, we have $k_I < 0$. Then, purely outgoing, exponentially increasing functions (resonant states) are defined by points in the fourth quadrant of the complex k -plane. As usual, $\epsilon_R = E$ will be called a resonance and $\Gamma = 2|\epsilon_I|$ the inverse of lifetime. We shall write $u(x, \epsilon = E - \frac{i}{2}\Gamma) \equiv \varphi_{\epsilon}(x)$.

Observe that density (12) increases exponentially for either large $|x|$ or large negative values of t . The usual interpretation is that the compound (φ_{ϵ}, V) represents a decaying system which emitted waves in the remote past $t - x/v$. As it is well known, the long lifetime limit ($\Gamma \rightarrow 0$) is useful to avoid some of the complications connected with the limit $t \rightarrow -\infty$ (see discussions on time asymmetry in [13]). In this context, we shall impose the condition:

$$\frac{\Gamma/2}{\Delta E} \ll 1. \quad (13)$$

Thus, the level width Γ is much smaller than the level spacing ΔE in such a way that closer resonances imply narrower widths (longer lifetimes). An additional condition which will be useful in the next calculations reads

$$E > \Delta E. \quad (14)$$

In general, the main difficulty is precisely to find the adequate E and Γ . However, for one-dimensional stationary short range potentials and appropriate values of V_0 and ζ , the transmission coefficient T presents a series of peaks. Each sharp peak is a bell-shaped curve of width Γ which can be described by the Fock-Breit-Wigner (FBW) distribution

$$\omega(\epsilon_R, E) = \frac{(\Gamma/2)^2}{(\epsilon_R - E)^2 + (\Gamma/2)^2}. \quad (15)$$

The center E of the peak defines a wave for which the scattering is ineffective (E is a transparency!). Energies ϵ_R which are very close to E , namely $|\epsilon_R - E| \leq \Gamma/2$, induce a resonance: the wave interacts with the potential in such a way that the time to cross the interaction zone is maximum. The superposition of a denumerable set of FBW distributions (each one centered at each resonance $E_n, n = 1, 2, \dots$) entails an approximation of the coefficient T such that the larger the number N of close resonances involved, the higher the precision of the approximation:

$$T \approx \omega_N(\epsilon_R) = \sum_{n=1}^N \omega(\epsilon_R, E_n). \quad (16)$$

The above description suggests a graphical method to calculate E and Γ (see Appendix A).

3 Darboux-Gamow transformations

In order to throw further light on the complex function β we may note that (2) transforms the Schrödinger equation (1) into a Riccati one

$$-\beta' + \beta^2 + \epsilon = V. \quad (17)$$

Remark that (17) is not invariant under a change in the sign of the superpotential β

$$\beta' + \beta^2 + \epsilon = V + 2\beta'. \quad (18)$$

These last equations define a Darboux transformation $\tilde{V} \equiv \tilde{V}(x, \epsilon)$ of the initial potential V . The Darboux-Gamow deformation is necessarily a complex function

$$\tilde{V} = V + 2\beta' \equiv V - 2\frac{d^2}{dx^2} \ln \varphi_\epsilon. \quad (19)$$

The solutions $y \equiv y(x, \epsilon, \mathcal{E})$ of the non-Hermitian Schrödinger equation

$$-y'' + \tilde{V}y = \mathcal{E}y \quad (20)$$

are easily obtained

$$y \propto \frac{W(\varphi_\epsilon, \psi)}{\varphi_\epsilon}, \quad (21)$$

where $W(*, *)$ stands for the Wronskian of the involved functions and ψ is eigensolution of (1) with eigenvalue \mathcal{E} .

Let us analyze the properties of these new solutions. First, if ψ_s is the scattering state of H connected with the positive kinetic parameter $\kappa = \sqrt{\mathcal{E}_s}$, equations (6) become

$$\psi_{s<} = e^{i\kappa x} + L_s e^{-i\kappa x}, \quad \psi_{s>} = S_s e^{i\kappa x} \quad (22)$$

where we have assumed a single source at the left of V . Hence, $T = |S_s|^2$ and $R = |L_s|^2$ are such that $R + T = 1$. The transformed scattering waves are obtained from (21) to read

$$y_{s<} = (\beta_{<} + i\kappa)e^{i\kappa x} + (\beta_{<} - i\kappa)L_s e^{-i\kappa x}, \quad y_{s>} = (\beta_{>} + i\kappa)S_s e^{i\kappa x}. \quad (23)$$

Hence, we have

$$\tilde{R} = |t|^2 R, \quad \tilde{T} = |t|^2 T, \quad t = \frac{\beta_{>} + i\kappa}{\beta_{<} + i\kappa}. \quad (24)$$

After using (11) and considering $\epsilon_R > 0$ we arrive at

$$\tilde{R} + \tilde{T} \approx \frac{1 + \left(\frac{v_s}{v}\right)^2 \left[1 - 2\frac{v}{v_s}\right]}{1 + \left(\frac{v_s}{v}\right)^2 \left[1 + 2\frac{v}{v_s}\right]} \quad (25)$$

where $v_s \neq 0$ and $v \neq 0$ are the flux velocities of the scattering wave ψ_s and the Gamow-Siegert function φ_ϵ respectively. Thereby, $\tilde{R} + \tilde{T} \approx 1$, no matter the value of $v_s/v \neq 1$. That is, scattering waves ψ_s and their Darboux-Gamow deformations y_s share similar transmission probabilities.

Now, let us suppose that Hamiltonian H includes a point spectrum $\sigma_d(H) \subset \text{Sp}(H)$. If ψ_n is a (square-integrable) eigenfunction with negative eigenvalue \mathcal{E}_n , then its Darboux-Gamow deformation (21) is bounded:

$$\lim_{x \rightarrow \pm\infty} y_n = \mp(\sqrt{\mathcal{E}_n} + ik) \left(\lim_{x \rightarrow \pm\infty} \psi_n \right). \quad (26)$$

Thereby, y_n is a normalizable eigenfunction of \tilde{H} with eigenvalue \mathcal{E}_n . However, as ϵ is complex, although the new functions $\{y_n\}$ may be normalizable, they will not form an orthogonal set [8] (see also [14] and the ‘puzzles’ with self orthogonal states [15]). There is still another bounded solution to be considered. Function $y_\epsilon \propto \varphi_\epsilon^{-1}$ fulfills equation (20) for the complex eigenvalue ϵ . Since $\lim_{x \rightarrow \pm\infty} |y_\epsilon|^2 = e^{\pm 2k_I x}$ and $k_I < 0$, we have another normalizable function to be added to the set $\{y_n\}$.

In summary, one is able to construct non-Hermitian Hamiltonians \tilde{H} for which the point spectrum is also $\sigma_d(H)$, extended by a single complex eigenvalue $\text{Sp}(\tilde{H}) = \text{Sp}(H) \cup \{\epsilon\}$.

3.1 New short range real potentials

The iteration of the previous procedure is easy once a set of Gamow-Siegert functions $\{\varphi_\epsilon\}$ belonging to the complex eigenvalues $\{\epsilon\}$ has been given:

$$V_2 = \tilde{V} + 2\beta'_2(\alpha) \quad (27)$$

where $\beta_2(\alpha) \equiv \beta(x, \epsilon, \alpha)$ is a Bäcklund-like function [16] defined by the finite-difference algorithm

$$\beta_2(\alpha) = -\beta(\epsilon) + \frac{\alpha - \epsilon}{\beta(\alpha) - \beta(\epsilon)} \quad (28)$$

and fulfilling

$$-\beta'_2(\alpha) + \beta_2^2(\alpha) + \alpha = \tilde{V}, \quad \alpha \in \mathbb{C}. \quad (29)$$

In general $V_2 \equiv V_2(x, \epsilon, \alpha)$ is complex; however, this becomes real if $\alpha = \bar{\epsilon}$ [7, 8]:

$$V_2 = V + 2 \left(\frac{\epsilon_I}{\beta_I} \right)' = V - 4 \left(\frac{\epsilon_I}{v} \right)' \quad (30)$$

and the new functions $\Psi \equiv \Psi(x, \epsilon, \mathcal{E})$, such that $H_2\Psi = \mathcal{E}\Psi$, read

$$\Psi = (\epsilon - \mathcal{E})\psi - 2 \left(\frac{\epsilon_I}{v} \right) y. \quad (31)$$

In this case, V_2 is a Hermitian short range potential and there is no additional eigenvalues. Hence, H_2 and H are strictly isospectral. A straightforward calculation shows that Darboux-Gamow deformations of $\psi_n \in L^2(\mathbb{R})$ correspond to normalizable Ψ_n while scattering states ψ_s are transformed into Ψ_s , with similar transmission probabilities.

In the next sections we shall deform the simplest short range one-dimensional potentials: square wells and barriers.

4 Square wells

Let us consider the square well potential

$$V(x) = -V_0 \Theta \left(\frac{b}{2} - |x| \right), \quad \Theta(x) = \begin{cases} 1, & x \geq 0 \\ 0, & x < 0 \end{cases} \quad (32)$$

with $V_0 > 0$ and $b > 0$. We shall assume that the only source of particles is at the left of the interaction zone (this arbitrariness is allowed by the parity symmetry of the potential). In this way, we shall analyze the scattering by an attractive potential of range b .

The scattering solution of the Schrödinger equation (1) for potential (32) reads:

$$u = \begin{cases} e^{ikx} + L(k)e^{-ikx}, & x < -\frac{b}{2} \\ \frac{k}{\Delta} e^{-ikb/2} \left[i(k \cos \frac{qb}{2} - iq \sin \frac{qb}{2}) \sin qx \right. \\ \quad \left. + (q \cos \frac{qb}{2} - ik \sin \frac{qb}{2}) \cos qx \right], & -\frac{b}{2} \leq x \leq \frac{b}{2} \\ S(k)e^{ikx}, & \frac{b}{2} < x \end{cases} \quad (33)$$

where

$$L(k) = i \left(\frac{V_0 \sin qb}{2\Delta} \right) e^{-ikb}, \quad S(k) = \left(\frac{kq}{\Delta} \right) e^{-ikb}. \quad (34)$$

The kinetic and interaction parameters are defined respectively by $k^2 = \epsilon$ and $q^2 = k^2 + V_0$, while Δ is the function

$$\Delta(k) = \left(k \cos \frac{qb}{2} - iq \sin \frac{qb}{2}\right) \left(q \cos \frac{qb}{2} - ik \sin \frac{qb}{2}\right). \quad (35)$$

Let us concentrate on the *transmission amplitude* S , which is regular in I_+ except for the points k_+ located on the positive imaginary axis (that is, each k_+ corresponds to a bound state, see Appendix A). It is simple to verify that k and $-\bar{k}$ will produce the same peaks in the transmission coefficient, that is, $\overline{S(k)} = S(-\bar{k})$. However, they are in I_- (as discussed in Section 2, k is in the fourth quadrant of the k -plane). Hence, S must be extended to be analytic in I_- . First, let us observe that the relationship

$$S(-k)S(k) = 1 \quad (36)$$

is fulfilled for the points k which are such that $qb = n\pi$. Since $-k \in I_+$, this last equation defines $S(k) = 1/S(-k)$ as an analytical function in I_- but at the points $-k$ which are zeros of S in I_+ . In a similar manner, we realize that $S(-\bar{k})$ is analytical in I_- except for the points \bar{k} which are zeros of S in I_+ . In summary, let k_n be a pole of S in the fourth quadrant of the k -plane, then $-\bar{k}_n$ is also a pole while \bar{k}_n and $-k_n$ are zeros of S . Thereby, S is a meromorphic function of k , with poles restricted to the positive imaginary axis (bound states) and the lower half-plane (resonances). On the other hand, if S is studied as a function of ϵ , it is necessary to consider a two-sheet Riemann surface ($k^2 = \epsilon$) with a cut along the positive real axis. Complex poles of $S(\epsilon)$ always arise in conjugate pairs (corresponding to k and $-\bar{k}$) while poles on the negative real axis correspond to either bound or antibound states.

4.1 Analytical approach for calculating resonances

In this section we shall derive expressions for the resonance E and the width Γ in terms of the potential parameters. We assume that the incoming kinetic parameter k is a complex number with nontrivial imaginary part. As the presence of the short range potential is necessarily encoded in the (complex) interaction parameter, most of the approximations will be made on q .

For complex q , additional to (10), the real and imaginary parts of ϵ read

$$E = q_R^2 - V_0 - q_I^2, \quad \frac{\Gamma}{2} = -2q_R q_I. \quad (37)$$

The combination of equations (37) leads to:

$$\frac{1}{4} \left(\frac{\Gamma}{2}\right)^2 \gamma^2 - (V_0 + E)\gamma - 1 = 0 \quad (38)$$

where $\gamma = q_I^{-2}$. Dropping the negative root we get

$$q_I^2 = \frac{\frac{1}{2}(\Gamma/2)^2}{(V_0 + E) \left(1 + \sqrt{1 + \frac{1}{4} \left(\frac{\Gamma/2}{V_0 + E}\right)^2}\right)}. \quad (39)$$

On the other hand, since $V_0 > 0$, condition (14) produces

$$\frac{\Gamma/2}{V_0 + E} < \frac{\Gamma/2}{E} < \frac{\Gamma/2}{\Delta E} \quad (40)$$

which, together with condition (13), implies

$$\left(\frac{\Gamma/2}{V_0 + E} \right)^2 \approx 0. \quad (41)$$

Hence, equation (39) gives

$$q_I \approx \frac{\Gamma}{4\sqrt{V_0 + E}}. \quad (42)$$

This value of q_I , when substituted into the expression for Γ in (37), leads to

$$E \approx q_R^2 - V_0. \quad (43)$$

We first notice that the positiveness of E is ensured whenever q_R fulfills $q_R^2 > V_0$. Now, a simple comparison between (43) and (37) shows that q_I^2 has to be smaller than V_0 . We then have a relation of order $q_I^2 < V_0 < q_R^2$. As we shall see, it is most convenient to constrain the values of q_R and q_I as weighted by the cutoff $b/2$:

$$\left(\frac{q_I b}{2\theta} \right)^2 < 1 < \left(\frac{q_R b}{2\theta} \right)^2, \quad \theta(V_0, b) := \frac{b}{2} \sqrt{V_0} \quad (44)$$

where we have introduced the parameter θ which encodes not only the range of application of our approach but the physical identity of the potential (32) as well.

Now, making the r.h.s. factor of (35) equal to zero, we obtain $q = \pm \sqrt{V_0} \sin \frac{qb}{2}$. After a straightforward calculation the corresponding equations for the real and imaginary parts are obtained. For $\theta \gg 1$ and small values of $\frac{qb}{2}$, the last one leads to $\cos \frac{q_R b}{2} \approx \mp \frac{1}{\theta}$. Therefore, we arrive at

$$\frac{q_R b}{2} \approx \frac{n\pi}{2} \pm \frac{1}{\theta} + \mathcal{O}\left(\frac{1}{\theta^3}\right) \quad (45)$$

where n is to be determined. After introducing (45) into (43), we finally get a discrete set of resonances

$$E \approx \left[\left(\frac{n\pi}{2\theta} \right)^2 - 1 \right] V_0, \quad \frac{n\pi}{2} > \theta, \quad n \in \mathbb{N}. \quad (46)$$

It is clear that n must exceed a minimum value to get a positive energy. Let us take $n := n_{\text{inf}} + m$, $m = 0, 1, \dots$, where n_{inf} is the ceiling function of $2\theta/\pi$, i.e., $n_{\text{inf}} = \lceil \frac{2\theta}{\pi} \rceil$. In this way, $E_{n_{\text{inf}}} \equiv E_0$ is the smallest positive energy in (46). Hence

$$E_m = \left(\left[\frac{(n_{\text{inf}} + m)\pi}{2\theta} \right]^2 - 1 \right) V_0, \quad m \in \mathbb{Z}^+. \quad (47)$$

The derivation of Γ is now easy. Making the l.h.s. of Δ equal to zero we arrive at $k_I = \pm\sqrt{V_0} \cos \frac{q_R b}{2} \cosh \frac{q_I b}{2}$. After using (45), for small $q_I b/2$ one obtains

$$-\frac{k_I b}{2} \approx 1 + \frac{1}{2} \left(\frac{q_I b}{2} \right)^2. \quad (48)$$

With this last result and (43) into (10), the energy E can be rewritten as

$$\left(\frac{k_R b}{2\theta} \right)^2 = \left(\frac{q_R b}{2\theta} \right)^2 + \left(\frac{q_I b}{2\theta} \right)^2 + \frac{1}{\theta} - 1 \quad (49)$$

the second additive term is smaller than the first one (see equation (44)) and $\theta^{-1} \ll 1$, so equation (49) reduces to $k_R \approx \pm\sqrt{E}$. The combined substitution of these last results into the expression for Γ in (10) gives

$$\frac{\Gamma}{2} \approx \frac{4}{b} \sqrt{E} = \frac{2v_+}{b} \quad (50)$$

where the terms which are proportional or greater than the square of $q_I b/2$ have been dropped (compare our results with those reported in e.g. [17]).

It is remarkable that Γ is proportional to v_+ . For a given value of b (θ fixed), a hasty incident particle spreads its peak in T by spending less time in the interaction zone. As a result, the peaks centered at hot resonant energies $v_+^2/2$ tend to lose the FBW shape by excessively overlapping the next ones. The long lifetime limit ($\Gamma \rightarrow 0$), applied for fixed values of θ , is then a good criterion to select velocities v_+ as well as potential parameters in order to obtain appropriate Gamow-Siegert functions for the square wells.

4.1.1 Fock-Breit-Wigner distributions

The above discussion considered a complex kinetic parameter with nontrivial imaginary part. As we have seen, approximations leading to E are also useful to get Γ in the long lifetime limit. Next, we are going to verify that E and Γ so derived correspond to the center and width of a FBW peak in the transmission coefficient T . It is convenient to rewrite the transmission amplitude (34) as follows

$$S(k) = \frac{e^{-ikb}}{\cos qb[1 - ig(k)]}, \quad g(k) = \left(\frac{k^2 + q^2}{2qk} \right) \tan qb. \quad (51)$$

Let us consider a small displacement δE from the resonance energy E_m along the real axis of the ϵ -plane. Kinetic and interaction parameters are mapped as $k \rightarrow k + \delta k$ and $q \rightarrow q + \frac{1}{2q}\delta E$ respectively. Near the resonance we get $qb \approx 2n\pi + \frac{b}{2q}\delta E$. Thus $g \approx (2/\Gamma_m)\delta E$, where we have used (50). Hence

$$S(k + \delta k) \approx \frac{e^{-i(k+\delta k-n\pi)b}}{1 - i2\delta E/\Gamma_m}$$

and finally we get

$$T(E_m + \delta E) \approx \frac{(\Gamma_m/2)^2}{(\Gamma_m/2)^2 + (\delta E)^2}. \quad (52)$$

This last expression is consistent with the previously defined FBW distribution (15) for small displacements along the real axis of the ϵ -plane, that is $\mathbb{R} \ni \delta E = (\epsilon_R - E_m)_{\epsilon_R \rightarrow E_m}$. A comparison of (47) and (50) with the results obtained from the graphical method is reported in Table 1 of Appendix A.

4.1.2 Diverse kinds of transformation function

Let us pay attention to solution (33) for a complex kinetic parameter k . Outside the interaction zone, it reads

$$u_{<} = e^{ik_{Rr}x} e^{-k_I x} + L(k) e^{-ik_{Rr}x} e^{k_I x}, \quad u_{>} = S(k) e^{ik_{Rr}x} e^{-k_I x}. \quad (53)$$

According with the discussion of the above sections, ‘decaying states’ $\varphi_\epsilon(x)$ correspond to kinetic parameters k living in the fourth quadrant of the complex plane (see Figure 1). The mirror images in the third quadrant $-\bar{k}$, give rise to ‘capture states’ $\varphi_{\bar{\epsilon}}$ behaving in the same global way as φ_ϵ (see equations (53)). On the other hand, equations (53) evaluated at \bar{k} correspond to an exponentially decreasing function (see Figure 2). The same is true for $-k$. We shall write $\varphi_{\bar{k}} \equiv u(x, \bar{k}^2)$. Although this solution reverts the decaying (12) to an exponentially growing dependence on time, it is useful for obtaining special cases of Darboux-Gamow deformations, as we are going to see.

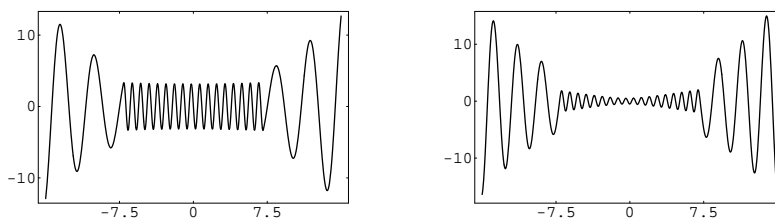


Figure 1: Real parts of the second (left) and third (right) decaying states of a square potential defined by $V_0 = 50$, $b = 14.2$. The Gamow-Siegert function φ_ϵ respectively belongs to the complex eigenvalues $\epsilon_1 = 3.3029 - i0.5119$ and $\epsilon_2 = 6.5823 - i0.7227$.

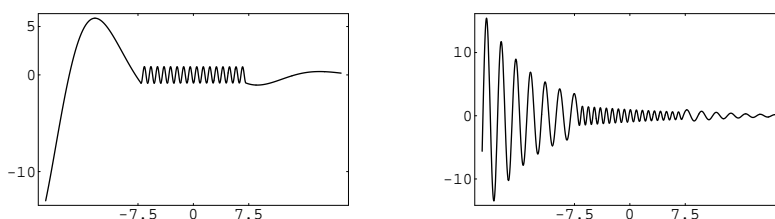


Figure 2: Imaginary parts of the first (left) and fourth (right) decreasing functions $\varphi_{\bar{k}}$ of the potential described in Figure 1. The complex kinetic parameters are respectively $\bar{k}_0 = 0.3072 + i0.2484$ and $\bar{k}_3 = 3.1496 + i0.2811$.

4.2 New complex and real wells

It is common to use complex potentials $V = V_R + iV_I$, $V_I = \text{const}$, for describing either absorption or emission of flux according with the sign of V_I (see e.g. [18]). In contrast, the case when V_I is an arbitrary function of the position is rarely analyzed because the related eigenvalue equation is involved. However, in Section 3 we realized that Darboux-Gamow deformations \tilde{V} are non-trivial exactly solvable complex potentials.

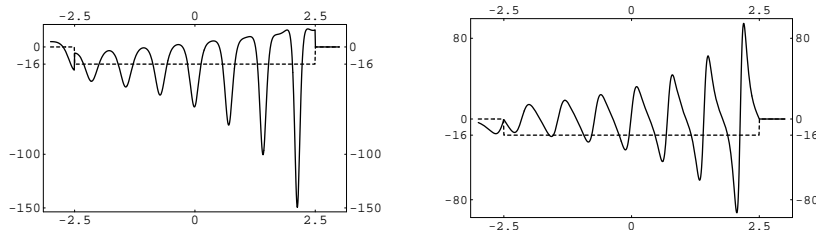


Figure 3: The real (left) and imaginary (right) parts of the Darboux-Gamow deformation \tilde{V} of a square well (dashed) for which $V_0 = 16$ and $b = 5$. The lowest decreasing function $\varphi_{\bar{k}}$ of the initial potential is the transformation function with $\bar{k}_0 = 1.7504 + i0.7657$.

A typical Darboux-Gamow deformation of the square well (32) is shown in Figure 3. First observe that the initial parity symmetry is now broken. It is also remarkable the presence of several local minima and maxima as well as multiple changes of sign in both functions \tilde{V}_R and \tilde{V}_I . In a simple optical model the incident beam crosses a sequence of ‘obstacles’ (potential’s maxima and minima), each one absorbing a fraction of the beam and performing some operations on the rest in such a way that the states are never mixed (see discussions on the optical bench in [10]). As a consequence, the ‘optical’ potential \tilde{V} is no longer self-adjoint and corresponds to an optical device which both refracts and absorbs light waves. Moreover, this non-Hermitian potential has a point spectrum and normalized eigenfunctions which inherit its broken parity symmetry (see Figure 4).

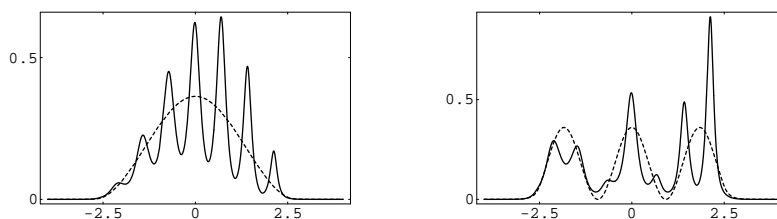


Figure 4: Left: The probability density belonging to the normalized ground state (dashed) of a square well potential ($V_0 = 16$, $b = 5$, see Figure 8) and its Darboux-Gamow deformation (continuous curve). The transformation parameters are the same as in Figure 3. Right: The related second excited states.

On the other hand, new real short range potentials are obtained by simultaneously using φ_ϵ and $\varphi_{\bar{\epsilon}}$ in (27)–(28). The result is illustrated in Figure 5 with a real potential V_2 for which $V_0 = 16$ and $b = 5$. It is notable that local deformations (that is, the number of maxima and minima) increases with the level of excitation of the transformation function.

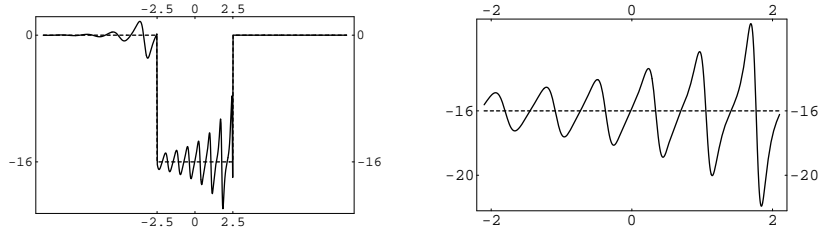


Figure 5: Twice Darboux-Gamow deformed square well potential ($V_0 = 16$, $b = 5$) for the same transformation parameters as in Figure 3. A detail of the bottom of this potential is shown at the right.

Finally, let us remark that, although our one-dimensional model is very simple, extensions to s-waves in three dimensions are immediate by properly selecting the odd solutions and adding to the initial potential an impenetrable wall along the negative axis.

5 Square barriers

The barrier potential ($V_0 > 0$)

$$V(x) = V_0 \Theta\left(\frac{b}{2} - |x|\right) \quad (54)$$

is usually studied as a special case of (32) for which the strength V_0 is allowed to be a negative number. Thus, kinetic and interaction parameters now read $k^2 = \epsilon$ and $q^2 = k^2 - V_0$. The involved solutions are then obtained by taking $V_0 \rightarrow -V_0$ and $\epsilon = E > 0$ in (33)–(35). However, a simple inspection of (47) and (50) shows that this is not the case in analyzing resonances (E_m and Γ_m are respectively negative and pure imaginary numbers if V_0 is simply negative!). In this section we shall obtain the appropriate expressions for the complex energies (10). As in the previous calculations, we look for the complex roots of $\Delta = 0$ fulfilling conditions (13) and (14). A straightforward calculation on the l.h.s. of (35) for the new k and q leads to

$$q_R = \pm \sqrt{V_0} \sin \frac{q_R b}{2} \sinh \frac{q_I b}{2}, \quad q_I = \pm \sqrt{V_0} \cos \frac{q_R b}{2} \cosh \frac{q_I b}{2}. \quad (55)$$

The smallness of the weighted q_I is now ensured by taking

$$\frac{q_R b}{2} = \frac{(2s+1)\pi}{2} + \delta, \quad s = 0, 1, 2, \dots \quad (56)$$

where δ is a slight perturbation of the weighted q_R . The introduction of (55) and (56) into the real and imaginary parts of ϵ (compare with equation (37)) gives

$$E_n \approx V_0 \left[\left(\frac{(2s+1)\pi}{2} \right)^2 + 1 \right], \quad \frac{\Gamma_s}{2} = \frac{2}{\theta} (E_s - V_0), \quad s = 0, 1, 2, \dots \quad (57)$$

In a similar form, the r.h.s. of equation (35) leads to expressions for E and Γ which are the same as (57) but they hold for semi-integer values of s . Thus we can write E_n and Γ_n with $n = 1, 2, 3, \dots$ such that $s = (n - 1)/2$. Therefore, $E_n > V_0$ for any integer $n \geq 1$. Moreover, Γ_n is always a positive number which grows as $n \rightarrow \infty$. Thus, resonant behaviour will be better distinguished, and it will have longer lifetime, for energies which are close to the top of the barrier. In other words, the resonance threshold is established by the strength of the potential (compare our results with those reported in e.g. [19]). In Table 2 of Appendix A we report a comparison of the results (57) with those obtained by means of the graphical method.

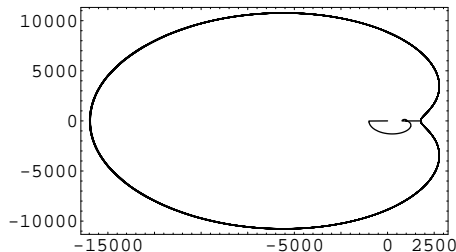


Figure 6: The Argand-Wessel diagram of the Darboux-Gamow deformed square barrier for $V_0 = 1000$, $b = 5$ and its first resonance (see Table 2). The external rings of this cardioid-like curve correspond to large negative values of the position x .

Figure 6 shows the Argand-Wessel diagram of the Darboux-Gamow deformation of a square barrier. The real and imaginary parts of this new potential show a series of maxima and minima which, in a similar manner as for the complex wells, can be modelled by the optical bench described in [10]. Once the method is iterated by means of $\varphi_{\bar{\epsilon}}$, the twice Darboux-Gamow deformed barriers are real. These new barriers present ‘hair’ over the top which induces stronger resonant phenomena (see Figure 7). Let us remark that the number of hairs increases with the excitation of the transformation function, just as it occurs for the nodes in bounded wavefunctions. Thus, the lowest resonance induces only one very localized distortion (a couple of hairs combed in opposite direction), the second one induces four hairs and so on. Observe also the global asymmetry of the new barriers, that is, $V_2(-x) \neq V_2(x)$. Finally, it is reasonable to assume that these haired barriers will induce delays on the scattering states which are longer than the delay produced by conventional square barriers (see simple models in [20]). The analysis of this phenomenon will be published elsewhere.

6 Concluding remarks

We have derived analytical expressions for the resonant energies of short range one-dimensional potentials in the long lifetime limit of the resonance levels. The same calculations leading to the ‘quantization’ E_m of the resonances are appropriate to obtain the corresponding lifetime inverses Γ_m . These results allowed the description of the transmission coefficient as a superposition of Fock-Breit-Wigner distributions, which is as good as

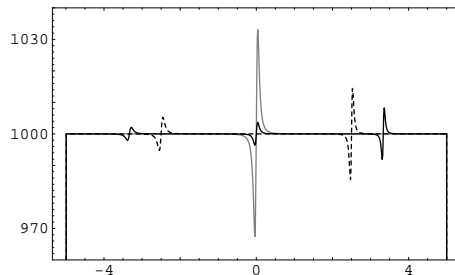


Figure 7: The top of twice Darboux-Gamow deformations of the square barrier $V_0 = 1000$, $b = 10$. The lowest decreasing function produces a very localized distortion (couple of ‘hairs’) on the new top (gray curve). The second (dotted curve) and third (solid curve) ones produce respectively two and three distortions (see Table 2 for specific values of the complex eigenvalues).

large is the number of resonances involved. Moreover, they also were used to transform Hermitian short range potentials into non-Hermitian ones which either preserve the initial energy spectra or include a complex eigenvalue with square-integrable eigenfunction. The new complex potentials are ‘opaque’ in the sense that they simultaneously emit and absorbs flux, just as an optical device which both refracts and absorbs light waves. The iteration of the method (ϵ and $\bar{\epsilon}$ combined) produces new real potentials for which the energy spectrum is exactly the same as the initial one.

The Darboux-Gamow deformations of square wells and square barriers have been presented as straightforward applications. In the first case, it has been shown that square-integrable eigenfunctions are mapped into square-integrable deformed eigenfunctions. In the second case we obtained ‘haired’ square barriers as a consequence of double Darboux-Gamow transformations. The hairs are very localized deformations on the top of the new barriers and are such that their number depends directly on the excitation of the involved transformation function. In all cases, the scattering states preserve their global properties after the deformations.

Some final comments would be important. Processes in which the incident wave falls upon a single scatterer are fundamental in the study of more involved interactions [21]. In general, for a single target the scattering amplitude is a function of two variables (e.g. energy and angular momentum). Our model corresponds to the situation in which one of the variables is held fixed (namely, the angular momentum). A more realistic three dimensional model is easily obtained from our results: even functions are dropped while an infinitely extended, impenetrable wall is added at the negative part of the straight line. Such a situation corresponds to s -waves interacting with a single, spherically symmetric, square scatterer (see e.g. [18]). On the other hand, the production of confined states within the continuum associated with lattice impurity (contact effect) has been recently reported in the context of Darboux-deformations [22]. Such a result indicates that our Darboux-Gamow approach can be extended to the case of spatially oscillating square well potentials. Then, the presence of ‘localized’ lattice deformations produced by resonant states could be in connection with the isolated transitions, observed in semiconductors, from a bound state within a quantum well to a bound state at an energy greater than the barrier height [23]. Work in this direction is in progress.

Acknowledgements

The support of CONACyT projects 24233-50766 and 49253-F is acknowledged.

Appendix A.

$V_0 = 1000, \quad b = 20, \quad n_{\text{inf}} = 202, \quad \epsilon = E_m - i\Gamma_m/2$		
Graphic	Analytical	
06.798680 - $i0.527888$	06.798344 - $i0.521472$	$m = 0$
16.790717 - $i0.843441$	16.791319 - $i0.819544$	$m = 1$
26.832718 - $i1.084738$	26.833641 - $i1.036023$	$m = 2$
36.926378 - $i1.295156$	36.925312 - $i1.215324$	$m = 3$
47.065373 - $i1.489006$	47.066330 - $i1.372098$	$m = 4$
57.258014 - $i1.673245$	57.256697 - $i1.513363$	$m = 5$
67.497189 - $i1.852008$	67.496412 - $i1.643124$	$m = 6$
77.786734 - $i2.028109$	77.785474 - $i1.763421$	$m = 7$
$V_0 = 743, \quad b = 22, \quad n_{\text{inf}} = 191, \quad \epsilon = E_m - i\Gamma_m/2$		
Graphic	Analytical	
00.911072 - $i0.174723$	00.911235 - $i0.173561$	$m = 0$
08.720839 - $i0.547966$	08.721274 - $i0.536941$	$m = 1$
16.571405 - $i0.768964$	16.572095 - $i0.740160$	$m = 2$
24.463107 - $i0.951658$	24.463700 - $i0.899287$	$m = 3$
32.397141 - $i1.116079$	32.396089 - $i1.034864$	$m = 4$
40.370347 - $i1.270414$	40.369261 - $i1.155214$	$m = 5$
48.381943 - $i1.419086$	48.383217 - $i1.264691$	$m = 6$
56.436735 - $i1.564930$	56.437956 - $i1.365912$	$m = 7$

Table 1: Representative numerical results for the resonance energies and widths of a square well. The potential parameters have been chosen such that the function $\omega_N(\epsilon_R)$ matches the transmission coefficient T , at least for the first 8 peaks.

The physical properties of the solution (33) are encoded in Δ . For example, the product $u\Delta$ makes evident that, after suppressing the incoming wave (i.e., $\Delta = 0$), still there are ‘reflected’ and ‘transmitted’ waves as well as a finite wave inside the interaction zone. Thus, the outgoing condition (7) is automatically satisfied. Moreover, since specific values of $k_+ = i\sqrt{|E|}$ produce both the quantization of $E < 0$ and the vanishing of the related solutions at $\pm\infty$, the usual interpretation of bound states as resonances with infinite lifetime ($\Gamma = 0$) is then recovered. Conventional expressions for these solutions are usually chosen to be simultaneously eigenstates of the parity operator, i.e. odd and even functions:

$$\psi_{\text{odd}}(x) = \begin{cases} \exp(\sqrt{|E|}x), & x < -\frac{b}{2} \\ -\left(\frac{\exp(-\frac{b}{2}\sqrt{|E|})}{\sin\frac{qb}{2}}\right) \sin qx, & -\frac{b}{2} \leq x \leq \frac{b}{2} \\ -\exp(-\sqrt{|E|}x), & \frac{b}{2} < x \end{cases} \quad (58)$$

$V_0 = 1000, \quad b = 5, \quad \epsilon = E_n - i\Gamma_n/2$		
Graphic	Analytical	
$1000.394784 - i0.009995$	$1000.394784 - i0.009987$	$n = 1$
$1001.579136 - i0.040036$	$1001.579136 - i0.039949$	$n = 2$
$1003.553057 - i0.090291$	$1003.553057 - i0.089886$	$n = 3$
$1006.316546 - i0.161043$	$1006.316546 - i0.159797$	$n = 4$
$1009.869604 - i0.252698$	$1009.869604 - i0.249683$	$n = 5$
$1014.212230 - i0.365794$	$1014.212230 - i0.359544$	$n = 6$
$1019.344424 - i0.501014$	$1019.344424 - i0.489379$	$n = 7$
$1025.266187 - i0.659204$	$1025.266187 - i0.639189$	$n = 8$
$V_0 = 1000, \quad b = 10, \quad \epsilon = E_n - i\Gamma_n/2$		
Graphic	Analytical	
$1000.098696 - i0.001248$	$1000.098696 - i0.001248$	$n = 1$
$1000.394784 - i0.004996$	$1000.394784 - i0.004993$	$n = 2$
$1000.888264 - i0.011248$	$1000.888264 - i0.011235$	$n = 3$
$1001.579136 - i0.020013$	$1001.579136 - i0.019974$	$n = 4$
$1002.467401 - i0.031303$	$1002.467401 - i0.031210$	$n = 5$
$1003.553057 - i0.045134$	$1003.553057 - i0.044943$	$n = 6$
$1004.836106 - i0.061525$	$1004.836106 - i0.061172$	$n = 7$
$1006.316546 - i0.080501$	$1006.316546 - i0.079898$	$n = 8$

Table 2: Representative numerical results for the resonance energies and widths of a square barrier. The potential parameters have been chosen such that the function $\omega_N(\epsilon_R)$ matches well the transmission coefficient T , at least for the first 8 peaks.

$$\psi_{\text{even}}(x) = \begin{cases} \exp(\sqrt{|E|} x), & x < -\frac{b}{2} \\ \left(\frac{\exp(-\frac{b}{2}\sqrt{|E|})}{\cos \frac{qb}{2}} \right) \cos qx, & -\frac{b}{2} \leq x \leq \frac{b}{2} \\ \exp(-\sqrt{|E|} x), & \frac{b}{2} < x \end{cases} \quad (59)$$

The energy eigenvalue conditions for these solutions are respectively

$$\cot \varrho = -\frac{\sqrt{\theta^2 - \varrho^2}}{\varrho}, \quad \tan \varrho = \frac{\sqrt{\theta^2 - \varrho^2}}{\varrho} \quad (60)$$

with θ defined in (44) and $\varrho = qb/2$. Figure 8 shows some of the first normalized eigenfunctions we are dealing with.

On the other hand, for one-dimensional short range potentials the transmission amplitude S could be interpreted as a 1×1 scattering matrix. So, to measure the cross section as a function of the energy of incoming particles corresponds to identify the local maxima of the transmission coefficient T . First, notice that a sharp peak of T can be connected with a Fock-Breit-Wigner distribution (15), just as it is illustrated in Figure 9. The peaks surrounded by a couple of local minima which are above $1/2$ will be dropped. The top of each of the included peaks, projected on the energy axis, defines a resonance. The width Γ of each peak is then defined by the distance between its right and left intersections with the horizontal at $1/2$. Function $\omega_N(\epsilon_R)$ in (16) includes N of these peaks, counted from left to right. In Figure 9 it is also shown a case for which the matching between T and

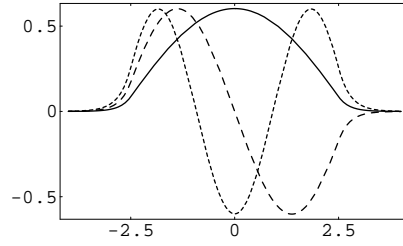


Figure 8: The ground state (continuous curve) and the first two excited bound states of a square well $V_0 = 16$, $b = 5$. The energies are respectively $\mathcal{E}_0 = -15.6379$, $\mathcal{E}_1 = -14.6983$, $\mathcal{E}_2 = -13.0812$.

ω_N is very good for the first ten resonances. Finally, Table 1 shows the results obtained with the graphical method as compared with the analytical procedure of Section 4 for the square well and different values of the range b and strength V_0 . Table 2 shows the corresponding results for the square barrier of Section 5.

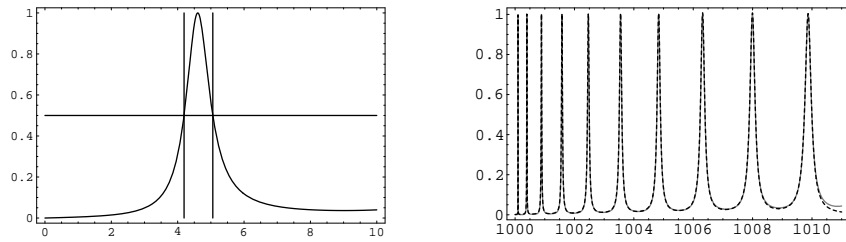


Figure 9: Left: First resonance of the square well $V_0 = 992.25$, $b = 20$. The graphic definition of the width Γ corresponds to the distance between the vertical lines centering the peak. Right: Functions T and ω_N (dotted curve) for the square barrier $V_0 = 10^3$, $b = 10$. In this case, the FBW sum matches well the transmission coefficient for the first ten resonances (see Table 2).

References

- [1] Gamov G, *Z Phys* **51** (1928) 204-212
- [2] Siegert AJF, *Phys Rev* **56** (1939) 750-752
- [3] Bohm A, Gadella M and Mainland GB, *Am J Phys* **57** (1989) 1103-1108;
Bohm A and Gadella M, *Lec. Notes in Phys.* vol 348 (New York: Springer 1989);
de la Madrid R and Gadella M, *Am J Phys* **70** (2002) 626-638
- [4] Civitarese O and Gadella M, *Phys Rep* **396** (2004) 41-113
- [5] Aguilar J and Combes JM, *Commun Math Phys* **22** (1971) 269-279;
Balslev E and Combes JM, *Commun Math Phys* **22** (1971) 280-294;
Simon B, *Commun Math Phys* **27** (1972) 1-9
- [6] Cannata F, Junker G and Trost J, *Phys Lett A* **246** (1998) 219-226;
Andrianov AA, Ioffe MV, Cannata F and Dedonder JP, *Int J Mod Phys A* **14** (1999) 2675-2688;
Bagchi B, Mallik S and Quesne C, *Int J Mod Phys A* **16** (2001) 2859-2872
- [7] Fernández DJ, Muñoz R and Ramos A, *Phys Lett A* **308** (2003) 11-16
- [8] Rosas-Ortiz O and Muñoz R, *J Phys A: Math Gen* **36** (2003) 8497-8506;
Rosas-Ortiz O, *Rev Mex Fís* **53 S2** (2007) 103-109 [arXiv:0810.2283v1 (quant-ph)]
- [9] Muñoz R, *Phys Lett A*, **345** (2005) 287-292;
Samsonov BF and Pupasov AM, *Phys Lett A* **356** (2006) 210-214;
Samsonov BF, *Phys Lett A* **358** (2006) 105-114
- [10] Mielnik B and Rosas-Ortiz O, *J Phys A: Math Gen* **37** (2004) 10007-10036
- [11] Fernández DJ and Rosu H, *Rev Mex Fís* **46 S2** (2000) 153-156
[arXiv:quant-ph/0102091v1];
Fernández DJ and Rosu H, *Phys Scr* **64** (2001) 177-183
- [12] Blatt JM and Weisskopf VF, *Theoretical Nuclear Physics* Wiley NY 1952
- [13] Bohm AR, Scurek R and Wikramasekara S, *Rev Mex Fís* **45 S2** (1999) 16-20
[arXiv:nucl-th/9902076v1]
- [14] Ramírez A and Mielnik B, *Rev Mex Fís* **49 S2** (2003) 130-133
[arXiv:quant-ph/0211048v1]
- [15] Sokolov AV, Andrianov AA and Cannata F, *J Phys A: Math Gen* **9** (2006) 10207-10227
- [16] Fernández DJ, Hussin V and Mielnik B, *Phys Lett A* **244** (1998) 309-316;
Mielnik B, Nieto LM and Rosas-Ortiz O, *Phys Lett A* **269** (2000) 70-78

- [17] Webber TA, Hammer CL and Zidell VS, *Am J Phys* **50** (1982) 839-845;
Sprung DWL and Wu H, *Am J Phys* **64** (1996) 136-144
- [18] Feshbach H, Porter CE and Weisskopf VF, *Phys Rev* **96** (1954) 448-464
- [19] Antoniou IE, Gadella M, Hernandez E, Jauregui A, Melnikov Y, Mondragón A and
Pronko GP, *Chaos, Sol. and Fractals* **12** (2001) 2719-2736;
de la Madrid R, *J Phys A: Math Gen* **37** (2004) 8129-8157
- [20] Moshinsky M, *Phys Rev* **84** (1951) 525-532;
Nussenzveig HM, *Phys Rev D* **6** (1972) 1534-1542;
García-Calderón G and Rubio A, *Phys Rev A* **55** (1997) 3361-3370
- [21] Nussenzveig HM, *Causality and Dispersion Relations* (Academic Press, NY 1972)
- [22] Fernández DJ, Mielnik B, Samsonov B and Rosas-Ortiz O, *J Phys A: Math Gen* **35**
(2002) 4279-4291;
Rosas-Ortiz O, *Rev Mex Fís* **49 S2** (2003) 145-147 [arXiv:quant-ph/0302189v2]
- [23] Capasso F, Sirtori C, Faist J, Sivco DL, Chu SNG and Cho AY, *Nature* **358** (1992)
565-567